Plasma surface modification of two-component composite scaffolds consisting of 3D-printed and electrospun fiber components from biodegradable PLGA and PLCL

Manasanan Namhongsa[a,b], Donraporn Daranarong[c], Robert Molloy[d], Sukunya Ross[e], Gareth M. Ross[e], Adisorn Tuantranont[f], Dheerawan Boonyawan[g], Jiraporn Tocharus[h], Sivanan Sivasinprasasn[i], Paul D. Topham[j], Brian J. Tighe[j] and Winita Punyodom[a,d]*

[a)] Department of Chemistry, Faculty of Science, Chiang Mai University, Chiang Mai 50200, Thailand

[b)] Graduate School, Chiang Mai University, Chiang Mai 50200, Thailand

[c)] Science and Technology Research Institute, Chiang Mai University, Chiang Mai 50200, Thailand

[d)] Center of Excellence in Materials Science and Technology, Chiang Mai University, Chiang Mai 50200, Thailand

[e)] Center of Excellence in Biomaterials, Department of Chemistry, Faculty of Science, Naresuan University, Phitsanulok 65000, Thailand

[f)] National Security and Dual-Use Technology Center, National Science and Technology Development Agency, Thailand

[g)] Department of Physics and Materials Science, Faculty of Science, Chiang Mai University, Chiang Mai 50200, Thailand

[h)] Department of Physiology, Faculty of Medicine, Chiang Mai University, Chiang Mai 50200, Thailand

[i)] Department of Anatomy, Faculty of Medicine, Chiang Mai University, Chiang Mai 50200, Thailand

[j)] Aston Institute of Materials Research, Aston University, Birmingham, United Kingdom

**Corresponding Author's E-mail: winita.punyodom@cmu.ac.th*

ABSTRACT

In this study, two-component, morphologically composite scaffolds consisting of a 3D-printed component and an electrospun fiber component were fabricated and treated with a nitrogen-argon (N_2-Ar) plasma to enhance their surface properties. The 3D-printed component provided mechanical strength, while the electrospun fibrous component acted as a mimic to the extracellular matrix to improve cell-substrate interactions. Two biodegradable polyesters, poly(L-lactide-*co*-*ε*-caprolactone) (PLCL) and poly(L-lactide-*co*-glycolide) (PLGA), were used to create the scaffolds. The resulting 3D/E/N_2-Ar scaffolds were characterized in terms of surface properties (morphology, chemical compositions, wettability, roughness, crystallinity), degradation, mechanical properties, and cell cytotoxicity, cell attachment and proliferation, LDH release and cell apoptosis. Results showed that the plasma treatment significantly increased the surface roughness, wettability, and hydrophilicity of the scaffolds. The 3D-printed component provided sufficient mechanical support, while the electrospun fiber component promoted cell attachment and proliferation. The water contact angle of the scaffolds was greatly reduced from 124.0 ± 1.8° (PLCL) and 119.6 ± 1.4° (PLGA), to 0° and persisted even after 168 days. Human Schwann cells (SCs) showed excellent viability on both 3D/E/N_2-Ar and 3D/E scaffolds were in excess of 95%. Cells cultivated on the 3D/E/N_2-Ar scaffolds, with higher surface roughness, displayed significant increase in attachment and proliferation and a higher presence of healthy cells when compared with untreated 3D/E scaffolds. Both PLCL and PLGA scaffolds showed potential for use in biomedical applications. Although PLGA performed slightly better in terms of cell behavior, PLCL exhibits a slower degradation rate and higher percentage of mechanical strain. These results demonstrate the potential of these designed scaffolds to support cell regeneration in clinically relevant devices such as nerve guide conduits and nerve protectant wraps.

GRAPHICAL ABSTRACT

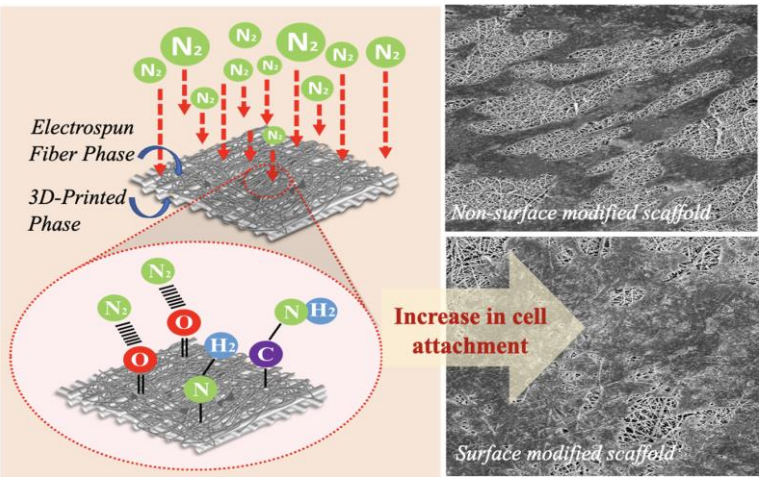

Keywords: Poly(L-lactide-*co*-ε-caprolactone); Poly(L-lactide-*co*-glycolide); 3D printing; electrospinning; Plasma surface modification

1. INTRODUCTION

Three-dimensional porous polymeric scaffolds have been extensively used in many biomedical applications such as surgical sutures, wound dressings, drug delivery carriers, bone fixation, and nerve guide conduits. Implantable scaffolds provide a suitable microenvironment for creating tissue or supporting cell regeneration to improve the function of damaged tissue and organs [1–5]. An ideal scaffold for tissue regeneration should have properties such as biodegradability, good biocompatibility, mimetic architecture for cell attachment, appropriate pore size for cell ingrowth and adequate diffusion of nutrients and oxygen to cells within the scaffold. At the same time, the scaffold must be of sufficient mechanical strength to maintain a stable architecture and prevent collapse during the regeneration process. Ongoing investigation into the discovery of optimal scaffolds persists, aiming to enhance the design of novel scaffolds via diverse materials and fabrication techniques. [6–10].

In term of materials used for polymeric scaffolds, aliphatic polyesters as resorbable materials have widespread use because of their biodegradability and biocompatibility [11–14]. These include poly(lactic acid) (PLA), poly(glycolic acid) (PGA), polycaprolactone (PCL), poly(L-lactide-*co*-ε-caprolactone) (PLCL) and poly(L-lactide-*co*-glycolide) (PLGA), as known synthetic biodegradable polymers that have acceptable biocompatibility, appropriate mechanical properties and tunable biodegradability with regulatory approval [2,15–16]. These materials are absorbed through hydrolysis degradation mechanisms in the body, demonstrating their negligible impact on usage [2,3]. Notwithstanding their numerous advantageous

properties, one of the primary drawbacks of these polymers lies in their hydrophobic nature, which stems from the presence of less polar functional groups in their molecular chains. This inherent characteristic impairs their compatibility with cells and consequently hinders cellular attachment and proliferation [7,17–19]. Consequently, in order to improve cell-substrate interactions and establish a better match with native tissue properties, researchers have focused on surface modifications of these polymers [13].

Numerous different surface modification methods have been applied to change surface properties (e.g. wettability, roughness and functional groups) of materials, including physical (e.g. plasma treatment, ultraviolet and laser treatment) and chemical (e.g. crosslinking, wet chemical and ‘‘click’’ chemistry) methods [20–23]. Among these approaches, plasma surface modification is a useful technique capable of modifying various surface-related properties of a material such as wettability, surface roughness, cell-substrate interactions via the introduction of new functional groups onto surfaces [24–29]. Gas plasmas are usually used in polymer plasma treatment, including nitrogen (N_2), oxygen (O_2), carbon dioxide (CO_2) and ammonia (NH_3). In these plasmas reactive sites such as nitrogen (-N_2), hydroxyl (-OH), carboxyl (-COOH), amino (-NH_2) groups can be generated on the surfaces of polymers [30]. In addition, some research has reported that inert gases such as argon (Ar), neon (Ne) and helium (He) can be utilized and mixed with other gases to enhance the concentration of active species through Penning excitation and ionization processes, leading to an increase in the desired groups or chains onto the surface of the material [29–32].

Various fabrication methods have been developed and implemented to produce polymeric scaffolds that meet the ideal criteria for tissue engineering. These methods include solvent casting, freeze-drying, electrospinning, micropatterning, and 3D printing [33]. Solvent casting is a cost-effective and straightforward technique for scaffold fabrication, but its drawbacks include the use of highly toxic solvents, poor interconnected pores with irregular shapes [33,34]. Electrospinning, on the other hand, has been widely used to create nano-scale fibers with architectures similar to the extracellular matrix (ECM), which enhances cell attachment and migration. However, the technique suffers from low reproducibility due to the random arrangement of fibers, limited scalability, and mechanical strength [35,36]. Among the various methods, 3D printing, such as fused deposition modeling (FDM), has gained widespread acceptance in medical device applications. This technique offers high degrees of shape freedom, controllable reproducibility, and mechanical strength but is limited in its ability to produce nanoscale resolution necessary for promoting cell attachment and proliferation [37].

Based on the advantages and disadvantages of the various fabrication techniques discussed, we set out to develop two-component composite scaffolds consisting of a 3D-printed and an electrospun fiber component (3D/E) in this study. These scaffolds consist of a 3D-printed supporting layer (3D phase) and an electrospun fiber layer (E phase) that serve as an ECM for cells to attach and migrate. The 3D phase provides mechanical strength, preventing the scaffold from collapsing during the regeneration process. To further enhance the efficiency of cell-substrate interaction, we employed plasma surface modification by N_2 and Ar.

To fabricate the 3D and E phases of our scaffolds, we chose medical-grade PLCL and PLGA produced in our Bioplastic Production Laboratory for Medical Applications at Chiang Mai University, Thailand (ASTM F1635-11 and ISO 10993-1). The ratios of 70:30 LA:CL for PLCL and 80:20 LA:GA for PLGA were utilized due to their favorable biological response in the body, appropriate mechanical properties, and tunable biodegradability, which can be adjusted by varying the ratios of LA:CL and LA:GA. Previous studies by our team have reported on the desirable characteristics of these polymers [2,3]. Although PLGA degrades faster than PLCL, which may be a concern in some clinical settings, PLCL is more mechanically flexible than PLGA, making both polymers viable options for our study.

We examined the effect of N_2-Ar plasma treatments on the surface properties, specifically the surface wettability, of the 3D/E scaffolds using various techniques, such as scanning electron microscopy (SEM), atomic force microscopy (AFM), X-ray photoelectron spectroscopy (XPS), and water contact angle (WCA). Additionally, we studied the absorption properties, *in vitro* degradation behavior, and cell viability of the scaffolds. We also evaluated cell-surface interactions through assays measuring cell proliferation, cell attachment, LDH release, and apoptosis. Our investigation aimed to provide insight into the potential of these scaffolds for use in tissue regenerative treatments, such as nerve guide conduits and ligament repair.

2. EXPERIMENTAL

2.1 Material

PLCL (70:30 mol%; M_n = 29,881 g mol^{-1}) and PLGA (80:20 mol%; M_n = 30,306 g mol^{-1}) pellets were synthesized by ring-opening bulk polymerization (ROP) and were supported by our Bioplastic Production Laboratory for Medical Applications, Chiang Mai

University (Thailand). Analytical grade dichloromethane (DCM), N,N-dimethylformamide (DMF) and chloroform ($CHCl_3$) were purchased from Labscan (Bangkok, THA). Dulbecco's Modified Eagle's Medium (DMEM), fetal bovine serum (FBS) and penicillin/streptococcus antibiotic were obtained from Thermo Fisher Scientific (Massachusetts, USA). Lactate dehydrogenase activity assay kit and annexin V-APC Assay Kit were purchased from Abcam (Cambridge, USA). Caspase-3 Activity Assay Kit was acquired from Elabscience (Texas, USA).

2.2 Preparation of 3D, 3D/E scaffolds

3D printed scaffolds (3D) fabricated by first dissolving PLCL (22.0% w/v) and PLGA (30.5% w/v) in chloroform. The resultant solution (~30 ml) was then loaded into the print cartridge of 3D-Bioplotter (EnvisionTEC, Gladbeck; Germany). The cartridge was placed in the low-temperature printing head and heated to maintain a temperature of 25.0 ± 0.1 ˚C. Bioplotter RP 3.1.1540 software was controlled for programming. A nitrogen pressure of 3.0 - 4.5 bar was applied onto the cartridge. The printing speed was controlled at 25 - 35 mm/s and the distance between the strands was set to 0.3 mm, calculated from the center of the strands. The layer thickness was adjusted to 0.32 mm, yielding a slight overlap. During the printing process the strand orientation was rotated by 0 and 90˚ [38–40].

An electrospun coating was then prepared on the 3D printed scaffolds (3D printed with electrospun fibers porous scaffolds (3D/E)). Spinning solutions of PLCL 10 % w/v and PLGA 14 % w/v were prepared by dissolving PLCL and PLGA pellets in a mixed-solvent system of dichloromethane and N,N-dimethylformamide in a ratio of 7:3 (% v/v) with vigorous stirring overnight. Before spin coating (on one-side), 3D printed scaffolds were mounted on aluminum foil as a ground collector. The spinning solution was then loaded into a 5 ml glass syringe equipped with a stainless-steel blunt-ended needle 20-gauge (outer diameter 0.91 mm) and delivered through a capillary. The spinning conditions were carefully controlled.The distance between the needle and the collector was 15 cm, the speed of the propulsion was 2 ml/h, the applied voltage was 15 kV, at a temperature of 25 °C and 30% relative humidity. Finally, electrospun fibers were collected onto the 3D printed scaffolds to achieve the 3D/E composite scaffolds. These 3D/E scaffolds were then dried in a vacuum oven at room temperature for 24 h to remove the residual solvent [41].

2.3 Plasma treatment of 3D/E scaffolds

Plasma treatment of PLCL and PLGA scaffolds was carried out using a lab-built 13.56 MHz inductively coupled plasma reactor with an N_2-Ar gaseous mixture. The ratio of N_2 to Ar was fixed at 10 % by volume, controlled at 0.03 and 0.10 Torr, respectively. Scaffolds (5 × 5 cm) were placed into the chamber of the plasma reactor which was then evacuated by a rotary pump to a base pressure of 2.2 Pa. The samples were first cleaned by Ar plasma sputtering for 10 min before treatment. The total pressure of the gas mixture was kept constant at 13.33 Pa. Samples were subsequently treated with N_2-Ar plasma discharge produced by a radio frequency (RF) generator working at powers of 50 and 100 W. Treatment time was varied for 1, 3, 5, 7 and 10 minutes [29,41].

2.4 Surface characterization

2.4.1 Surface morphology

The surface morphologies of the treated scaffolds were characterized by scanning electron microscopy (SEM, JEOL 5910 LV). Prior to SEM examination, the scaffolds were mounted onto SEM stubs using carbon tabs; the stub surfaces were then sputter-coated with gold at an acceleration voltage of 15 kV. The average pore sizes were assessed by the average width of gaps between fibers, in which 50 fibers were analyzed using image analysis software (ImageJ, National Institutes of Health, USA) from a random sampling of 50 fibers per SEM image.

2.4.2 Surface chemical composition

X-ray photoelectron spectroscopy (XPS) was used to analyze the qualitative elemental surface composition of untreated and treated scaffolds. An analysis of XPS spectra was acquired using a monochromated Al Kα source (energy of 1486.68 eV). The UV source was HeI (energy of 21.2 eV) and HeII (energy of 40.8 eV). A take-off angle of 90° between the sample and analyzer was used with a pass energy of 20 eV. High-resolution elemental scans of C_{1s} and N_{1s} were performed and curve-fitting was carried out using XPSPEAK software to analyze the chemical bonding state.

2.4.3 Wettability properties

After the plasma treatment, the surface wettability of untreated and treated PLCL and PLGA scaffolds was evaluated by static water contact angle meter (WCA, Homemade contact angle meter). A water droplet with a volume of 10 μL was placed using a microsyringe onto the scaffold specimens, which had been cut into 1 × 1 cm^2. The contact angles of the droplets were observed immediately after the plasma treatment and allowed to rest for 5 s on the scaffold. The image of the water droplet was observed using image analyzing software to determine the contact angle. The contact angle was measured five times at different locations and an average value was calculated (n=5).

To evaluate the absorptivity, a water droplet with a volume of 10 μL placed on the surface of each scaffold, was observed after 0, 1, 3, 5, 7, 14, 21, 28, 56, 84, 112, 140 and 168 days. The stabilized shape of the water droplet on the surface at each elapsed time point was recorded immediately after the water droplet was placed on surfaces. Averages and standard deviations of these measurements were also calculated for each sample (n=5).

2.4.4 Surface roughness

Atomic force microscopy (AFM) was also used before and after plasma treatments to determine the topographical changes on a nanoscale making use of the XE-70 atomic force microscope (Park Systems) operating in non-contact mode with a silicon cantilever (Nanosensors™ PPP-NCHR). Two-dimensional images of 15 × 15 μm^2 were recorded and analyzed using XEP software (v1.8.0), which allowed conversion to three-dimensional images. After an autofit of the X-Y plane, qualitative fiber roughness is determined by averaging out four random measurement values for each condition.

2.4.5 Crystallinity

The crystallinity of untreated and treated scaffolds was investigated by X-ray diffraction (XRD) (Rigaku MiniFlex 600) with a diffraction angle range (2θ) from 5° to 35° (Cu Kα, 1.54 Å).

2.5 *In vitro* hydrolytic degradation

Untreated and treated samples (1 × 1 cm^2) were fully immersed in a phosphate buffer saline (PBS) at pH 7.40 ± 0.01 and incubated at 37.0 ± 0.1 °C for 0, 1, 3, 5, 7, 14, 21, 28, 56, 84, 112, 140 and 168 days. The degradation solution was replaced with fresh media every week.

At predetermined time points, samples were withdrawn, washed with deionized water, and vacuum-dried to constant weight. *In vitro* hydrolytic degradation was determined by % weight retention. The weight retention of each sample was calculated by the following equation:

$$\%\, weight\ retention\ = \frac{w_t}{w_0} \times 100\%$$

where w_0 and w_t are the initial and final weight of PLCL and PLGA scaffolds, respectively.

2.6 Mechanical properties

Tensile tests were performed using a universal testing machine (Lloyd Instruments/Ametek LS2.5, AMETEK, Berwyn, USA, fitted with a 10 N load cell) to determine tensile stress-strain curves and Young's moduli. An elongation rate of 10 mm/min together with a 50 mm gauge length was used. The scaffolds were cut into rectangular stripes with a width of 10 mm and a length of 70.0 cm. Five replicates of all samples were tested and the average values reported.

2.7 MTT viability

The cytocompatibility of scaffolds was assessed using an MTT (3-(4,5-dimethylthiazol-2-yl)-2,5-diphenyl tetrazolium bromide) assay using a standard ISO-10993-5 protocol (ISO 10993-5:2009 Biological evaluation of medical devices - Part 5: Tests for *in vitro* cytotoxicity). Because one potential application for our composite systems is nerve guides we used Human Schwann Cells (SCs), which are the most widely used support cells in peripheral nerve regeneration [42,43]. SCs were obtained from ATCC (Virginia, USA).

The 96-well plate was contained with blank, positive control, and scaffold in serum-containing Dulbecco's Modified Eagle's Medium (DMEM) and maintained in a humidified atmosphere with 95 ± 5% humidity and 5% CO_2 for 24 ± 2 hours. This medium (extract medium) was replaced into another 96-well plate that contained cultured SCs cells and left at 37.0 ±1°C for 24 ± 2 hours. After incubation, the medium was removed and then MTT solution was added into the wells, following with another incubation at 37.0 ±1°C for 24 ± 2 hours. Then MTT solution was removed before added DMSO solution in each well to dissolve the MTT formazan purple crystals. This solution was determined its absorbance at 570 nm using Microplate reader (Anthos2010). At the step of preparation of cultured SCs cells, SCs at a cell density of 1×10^4 cells/mL were suspended in DMEM and maintained in a humidified

atmosphere with 95 ± 5% humidity and 5% CO_2 at 37.0 ±1°C for 24 ± 2 hours. The cultured medium was removed from the cultured SCs cells before the addition of extract medium.

2.8 Cell attachment and cell proliferation

The cell attachment and cell proliferation of SCs were analyzed using MTT assay. 2×10^4 cells of SCs were seeded on the samples and then cultured at 37.0 ± 1°C under 5 ± 0.1 % CO_2 and 95 ± 5% relative humidity, for 1, 3, 5 and 7 days. The medium was replaced every 3 days. After each time point, the cell attachment was observed by SEM. All scaffolds were prepared and fixed with fixative solution for overnight. After the fixation step, the scaffolds were washed with washing solution and stored for overnight. Then, each scaffold was immersed in various concentrations of ethanol solutions (20, 30, 40, 50, 60, 70 and 100% v/v) for 15 min and then dehydrated by Automated critical point dryer. Finally, the upper surface of each scaffold was coated by gold for SEM analysis to monitor cell attachment. For cell proliferation, after each time point, the incubated cells were stained with MTT at the concentration of 0.5 mg/mL in DMEM medium and incubated further for 2 h. After cells staining, MTT was removed and then 200 µL of DMSO was added in each well. Finally, 100 µL of dye solution was transferred into 96-well plate and the absorbance was measured using Microplate reader at 570 nm (Synergy H1, BioTek).

2.9 LDH assay

The effect of each scaffold on cell membrane integrity (both PLCL and PLGA) were assessed through the leakage of lactate dehydrogenase (LDH) after 1, 3 and 7 days of culture using LDH activity assay kit (MAK066, Sigma-Aldrich). SCs (*ca* $1x10^6$ cells) were suspended in DMEM-10% FBS completed medium and plated into 96-well plates with each scaffold (37 °C with 5% CO_2). After each time point, the samples were washed with cold LDH assay buffer and centrifuged (10,000 × *g*, 15 min, 4 °C). 25 µL sample of the supernatant was then transferred to a sterile 96-well plate and adjusted to a final volume of 50 µL with LDH assay buffer. 50 µL master reaction mixture was added into each well and thoroughly mixed. LDH analyses were performed at 450 nm using a microplate spectrophotometer (Synergy H1, BioTek).

2.10 Apoptosis assay

Cell apoptosis and death of SCs on scaffolds (both PLCL and PLGA) was measured using Annexin V-APC apoptosis assay kit (ab236215, Abcam). SCs were suspended in DMEM-10% FBS completed medium and plated into 96-well plates with each scaffold. The cells were cultured and incubated at 37.0 ± 1.0°C, 5 ± 0.1% CO_2, and 95 ± 5% relative humidity for 7 days. After cultivation, SCs (*ca* 1-5 × 10^6 cells) were harvested by trypsinization, counted, and plated into each well. SCs were centrifuged (400 × g, 5 min) and were washed with 1 × binding buffer before centrifuged (1,500 × g, 5 min). The cells were resuspended in Annexin V-APC/DAPI staining solution and incubated in the dark at room temperature for 10 min. Subsequently, cells were centrifuged (400 × g, 5 min) and discarded the supernatant and then added PBS (200 μL). Finally, all samples were analyzed using a microplate spectrophotometer (Synergy H1, BioTek) at 633 nm excitation and 700 nm emission for APC and 350 nm excitation and 450 nm emission for DAPI.

2.11 Caspase-3 assay

Caspase-3 enzyme activity was measured using caspase-3 activity colorimetric assay kit (E-CK-A311, Elabscience). SCs were suspended in DMEM-10% FBS completed medium and plated into 96-well plates with each scaffold. The cells were cultured and incubated at 37.0 ± 1.0 °C, 5 ± 0.1% CO_2, and 95 ± 5% relative humidity for 7 days. After cultivation, the cells were harvested by trypsinization, and counted. After resuspension with PBS, the cells were counted and centrifuged at 2,000 rpm for 5 min and then discarded the supernatant. An amount of 50 μL of cold lysis buffer working solution was added to each 2 × 10^6 cell/mL and incubated in ice bath for with oscillate 3 to 4 times during incubation. The cells were transferred to Eppendorf tube and centrifuged (12,000 × g, 15 min, 4 °C). Then, 2 × Reaction working solution (50 μL) and Ac-DEVD-pNA (5 μL) were added to the supernatant (45 μL) and incubated at 37 °C until the color changes obviously. The activity of caspase-3 in each sample solution was analyzed at 405 nm wavelengths using a microplate spectrophotometer (Synergy H1, BioTek).

2.12 Statistical analysis

All data was statistically evaluated using the two-way ANOVA analysis and Bonferroni post-test (significance level: <0.05).

3. RESULTS AND DISCUSSION

The present study introduces the development and fabrication of two-component composite scaffolds consisting of a 3D-printed and an electrospun fiber component (3D/E) using a combination of 3D printing and electrospinning techniques. To enhance the surface properties and cell-substrate interaction, plasma surface modification by N_2-Ar was employed. The 3D phase (Fig. 1a) acted as a supportive layer, while the E phase was utilized as an ECM (Fig. 1b) to improve cell attachment and proliferation. The N_2-Ar gaseous mixture was used to modify the scaffold surface (Fig. 1c). The optimal conditions for scaffold fabrication and surface modification were determined and the impact of plasma surface treatment on scaffold characteristics (morphology, crystallinity, and mechanical properties) and cell-substrate interaction (cytotoxicity, adhesion, proliferation, apoptosis, and caspase-3 enzyme activity) were investigated.

3.1 3D/E scaffolds: fabrication and characterization

The 3D and 3D/E scaffolds of PLCL and PLGA were successfully fabricated (Fig. 1a and b). Both 3D phases of PLCL and PLGA were transparent and had uniformly oriented channels and pores with mean diameters of 165 ± 5 and 215 ± 4 μm, respectively (Fig. 1a), whereas, the E phases were white and opaque (Fig. 1b). The cross-sectioned SEM images of 3D/E scaffolds clearly showed two different phases of 3D and electrospun fibers. The E phases of PLCL and PLGA had similar average pore sizes (0.289 ± 0.079 μm for PLCL and 0.287 ± 0.095 μm for PLGA). The average thicknesses of 3D/E scaffolds of PLCL (0.239 ± 0.002 mm) was slightly smaller than in that of PLGA (0.282 ± 0.005 mm).

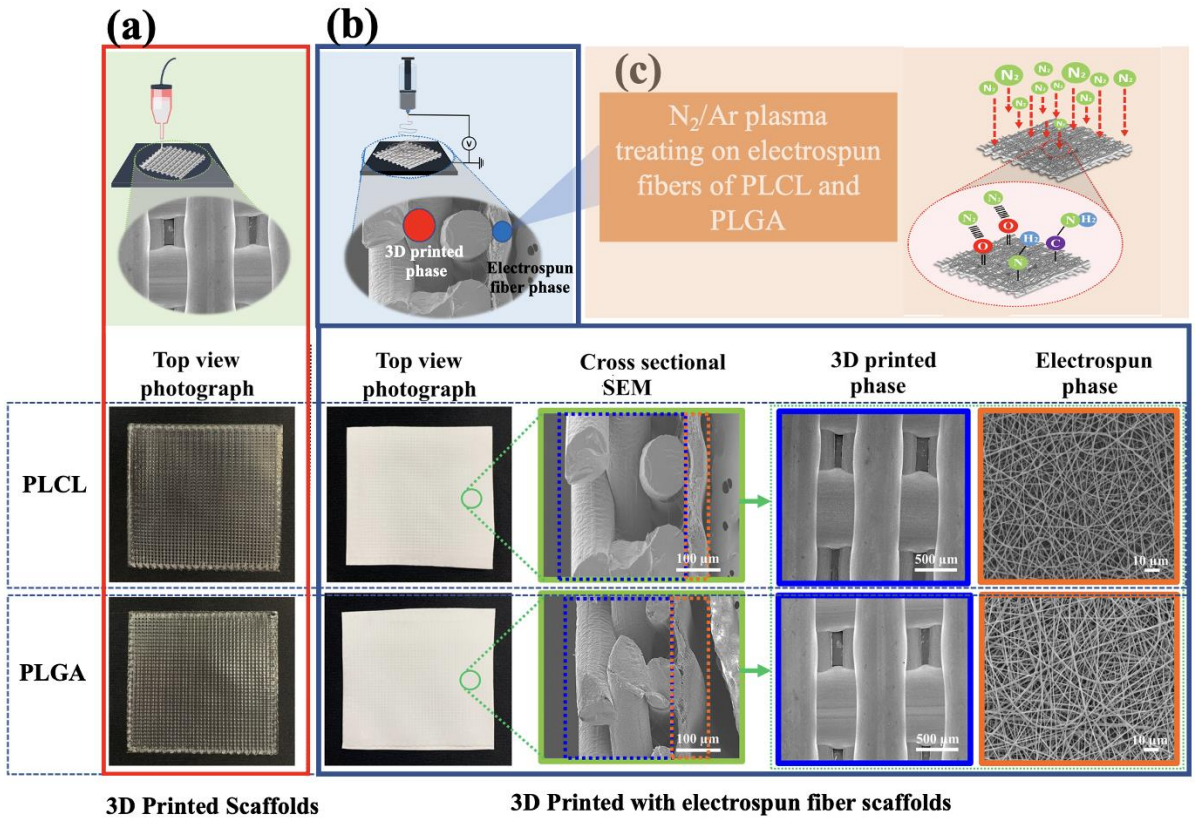

Fig. 1. Cartoon schematics, photographs and SEM images of (a) 3D printed component (3D) and (b) electrospun scaffold (E) of the PLCL (top) and PLGA (bottom) systems. (c) shows a cartoon illustration of the effect of plasma treatment on the scaffolds.

3.2 Optimization and characterization of the surface modification

3.2.1 Surface morphological analysis

Following surface modification of 3D/E scaffolds with N_2-Ar plasma at various treatment powers and times, the physical appearances and SEM images were analyzed, as shown in Fig. 2. The untreated scaffolds exhibited a smooth and flat mat. At an RF power of 50 W, the PLCL and PLGA scaffolds still exhibited a smooth and flat mat in optical images, while fibers merged when longer treatment times were applied, as observed in SEM images. At an RF power of 100 W, the scaffolds showed more deformation from a flat to curled mats in optical images, and fibers merged with longer treatment times, particularly for the PLGA scaffolds. The surfaces of the fibers were damaged due to the high energy acquired by the ions, as is generally known [44,45]. Consequently, the effect of N_2/Ar treatment with an RF power

of 50 W and different treatment times of 1, 3, 5, 7, and 10 mins was selected for further investigation.

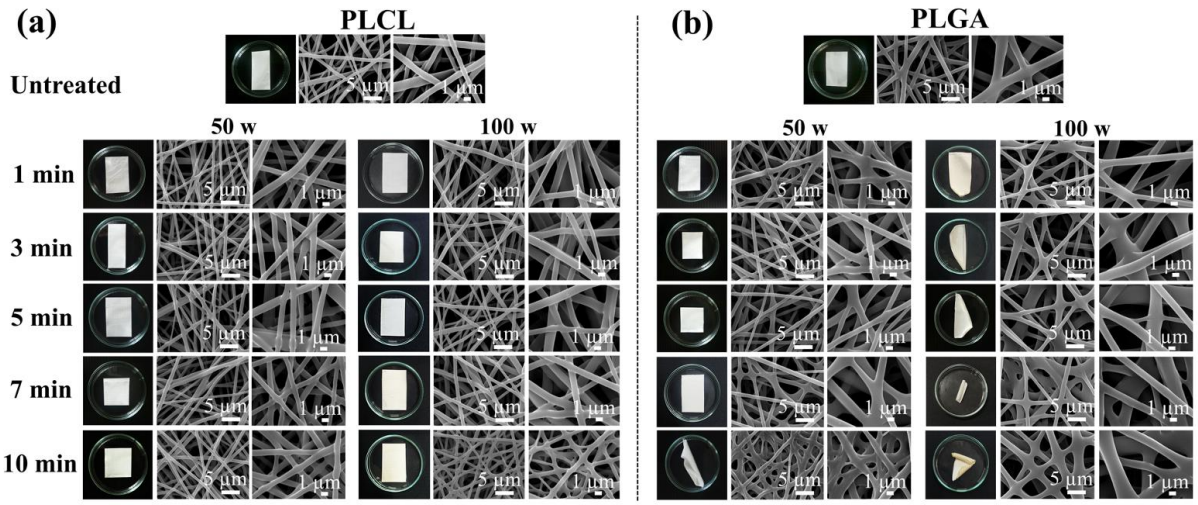

Fig. 2. Photographs and SEM images (at magnification of 5K and 10K (scale bar of 5 µm and 1 µm, respectively) of untreated and treated scaffolds by N_2-Ar; (a) PLCL and (b) PLGA, at different RF powers (50 and 100 W) and treatment times (1, 3, 5, 7 and 10 mins).

3.2.2 Wettability and surface chemical analysis

The surface wettability (Fig. 3a) and surface chemical compositions (Fig. 3b) of untreated and treated PLCL and PLGA scaffolds were analyzed by water contact angle and XPS. The contact angles of untreated scaffolds were observed to be 124.0 ± 1.8° (PLCL) and 119.6 ± 1.4° (PLGA), whereas the contact angle for all treated scaffolds decreased to 0°. XPS analysis revealed the presence of carbon (C_{1s}), nitrogen (N_{1s}), and oxygen (O_{1s}) peaks at 286.0, 400.0, and 532.0 eV, respectively. The N_{1s} peaks were observed on the treated scaffolds due to the N_2/Ar plasma treatment, while no N_{1s} peak was observed on the untreated scaffolds.

The dramatic reduction in static water contact angle (strictly, equilibrium advancing contact angles) is, perhaps, at first sight confusing. The clue to the underlying reason lies in the initial contact angles (i.e before plasma treatment). Our recorded values for PCL and PGLA (>>120^o) are significantly higher than those observed for these polymers in the literature (which are conventionally measured on smooth surfaces and are typically less than 100 ^{o}) [46-48] Similarly, the effects of various plasma treatments on a wide range of polymers will commonly lead to decreases in static contact angle of 40 - 80^o whereas our results show decreases in the region of 120^o · The reason for this very marked difference can be best

understood in the analysis of surface roughness effects which has been extensively and clearly expounded in standard texts [49-51].

Essentially, the very high initial contact angle that we observed is due to the porosity of our system and consequent entrapped air. The plasma treatment enhances surface wettability which means that the liquid now wets the surface rather than "riding on" entrapped air. This can be described as the transition from a Cassie-Baxter model to a Wenzel model [49-51] and leads to an enhancement in observed numerical contact angle reduction.

Our observations of the changes brought about by plasma treatment are consistent with the well-established principles based on the work of many researchers [52-56]. In summary, inert gas plasma irradiation creates stable free radicals on a polymer surface, which are able to react subsequently with atmospheric oxygen. Chain scission occurs more markedly in the less resistant amorphous regions than crystalline regions, leading to chain scission in the amorphous regions and a consequent increase in % crystallinity. Nitrogen is a relatively reactive plasma component, leading to an increase in nitrogen-containing groups in the polymer surface, quite independently of macroradical effects. Surface analysis by XPS has many advantages in surface analysis of plasma-treated surfaces because its nanometre-level penetration depth detects changes after short treatment times.

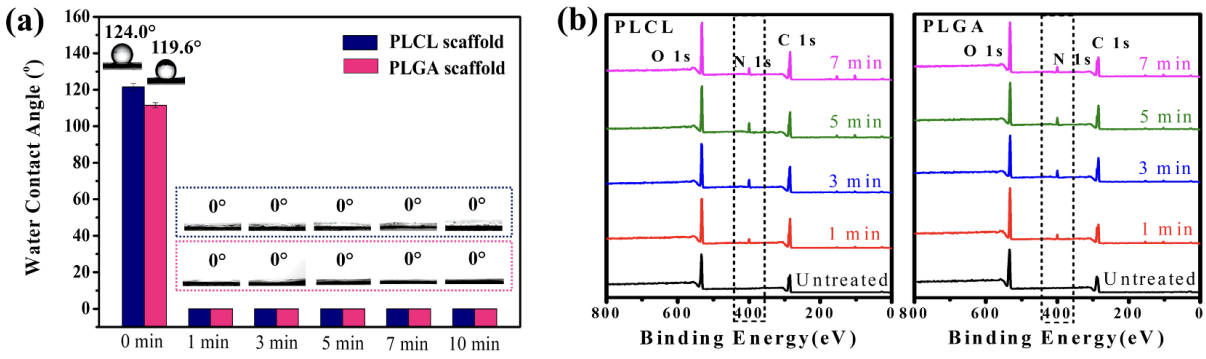

Fig. 3. Untreated and treated PLCL and PLGA scaffolds: **(a)** static water contact angle and sliding angle data, at RF power of 50 W with different treatment times (1, 3, 5, 7 and 10 mins) and **(b)** XPS survey spectra of untreated and treated PLCL and PLGA scaffolds, at RF power of 50 W with different treatment times (1, 3, 5 and 7 mins).

3.2.3 Indirect *in vitro* cytotoxicity

The percentages of viable Human Schwann Cells (SCs) on the untreated and treated PLCL and PLGA scaffolds with various N_2-Ar plasma treatment times of 1, 3, 5 and 7 minutes were assessed (Fig. 4). It was observed that the scaffolds at 3 min of N_2-Ar plasma treatment displayed the highest percentage of viable cells on the surfaces when compared with other treatment times (PLCL 96% ± 1.27, PLGA 96% ± 3.71). This result indicates that the scaffolds treated at 3 min were non-toxic to the cells (according to the ISO 10993-5:2009(E) standard, i.e. >70% viability). However, the plasma treated PLCL and PLGA scaffolds at 1 minute showed the lowest cell viability when compared with the control group and untreated scaffolds. Longer time treatment (at 5 and 7 min) decreases cell viability for both PLCL and PLGA scaffolds [57,58]. The decrease in cell viability of treated PLCL and PLGA scaffolds at 1, 5 and 7 minutes of plasma treatment might lead to induce cell oxidative stress, mitochondrial dysfunction and apoptosis as well as DNA damage [59,60].

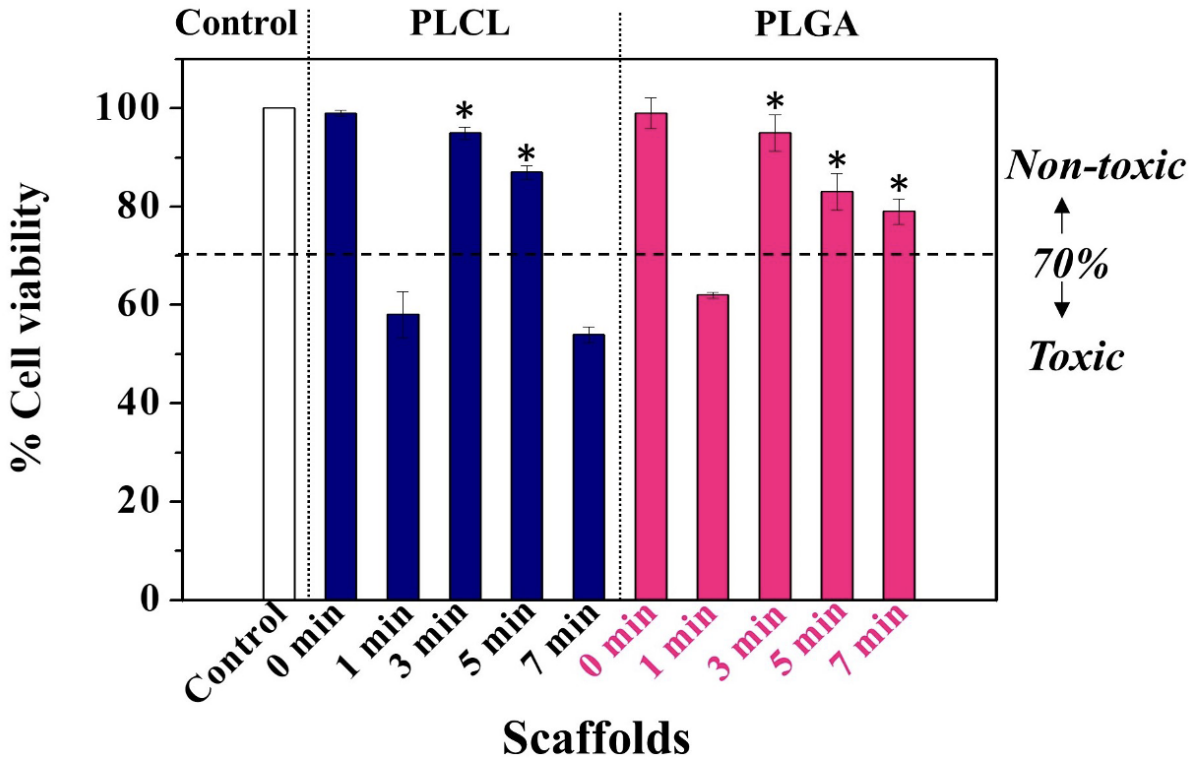

Fig. 4. Indirect *in vitro* cytotoxicity of SCs on scaffolds after 24 h of the MTT assay (*P < 0.05 compared with control), at 50 W with plasma treated for 1, 3, 5 and 7 min.

Among all plasma treated PLCL and PLGA scaffolds, the scaffolds at plasma treatment of RF generator working at 50 W for 3 minutes demonstrated the highest percentage of viable cells, therefore, they were chosen to study further in terms of the effect of surface properties, mechanical properties, storage times and biocompatibility test.

3.3 Scaffolds at N_2-Ar plasma treatment (RF powers of 50 W with 3 min)

3.3.1 Morphology, wettability, topography changes, crystallinity and surface chemical analysis

PLCL and PLGA scaffolds under our perceived optimum treatment conditions (RF power of 50 W with 3 min treatment) were white and opaque with thicknesses of 0.253 ± 0.002 and 0.266 ± 0.007 mm, respectively (see Fig. 2). The E phase of plasma-treated PLCL and PLGA scaffolds had the appearance of fibers with interconnected pores of 0.253 ± 0.016 and 0.238 ± 0.025 μm, respectively, and with mean diameters of 339 ± 22 nm and 662 ± 29 nm, respectively. PLCL- and PLGA-treated scaffolds both showed similar thickness and pore size after the plasma treatment. Measurements of changes in the surface hydrophilicity by static contact angle before and after modification, showed that the water drops on treated scaffolds were absorbed within 3 seconds (contact angles near 0°, Fig. 5a), indicating that the surface hydrophilicity of the scaffolds was improved [61]. Besides SEM imaging, AFM was also used to evaluate plasma influence of surface topography. The AFM images and the roughness values of untreated and treated for PLCL and PLGA scaffolds are shown in Fig. 5b. The treated scaffolds showed increases in roughness values from 229.75 nm to 306.54 nm for PLCL and from 198.95 nm to 374.43 nm for PLGA, when compared with untreated scaffolds which had "smooth" surfaces.

In addition, the crystallinity of both untreated and treated PLCL and PLGA scaffolds were studied by XRD (Fig. 5c). For untreated scaffolds, PLCL showed sharp crystalline peak at 2θ values of 14.9°, while PLGA showed a broad amorphous peak at 10°–25°. After plasma treatment, the PLCL scaffold showed an increase in crystalline peak intensity from 28.0% to 44.7% when compared with the untreated scaffold. However, the PLGA scaffold was substantially amorphous both before and after N_2-Ar plasma treatment.

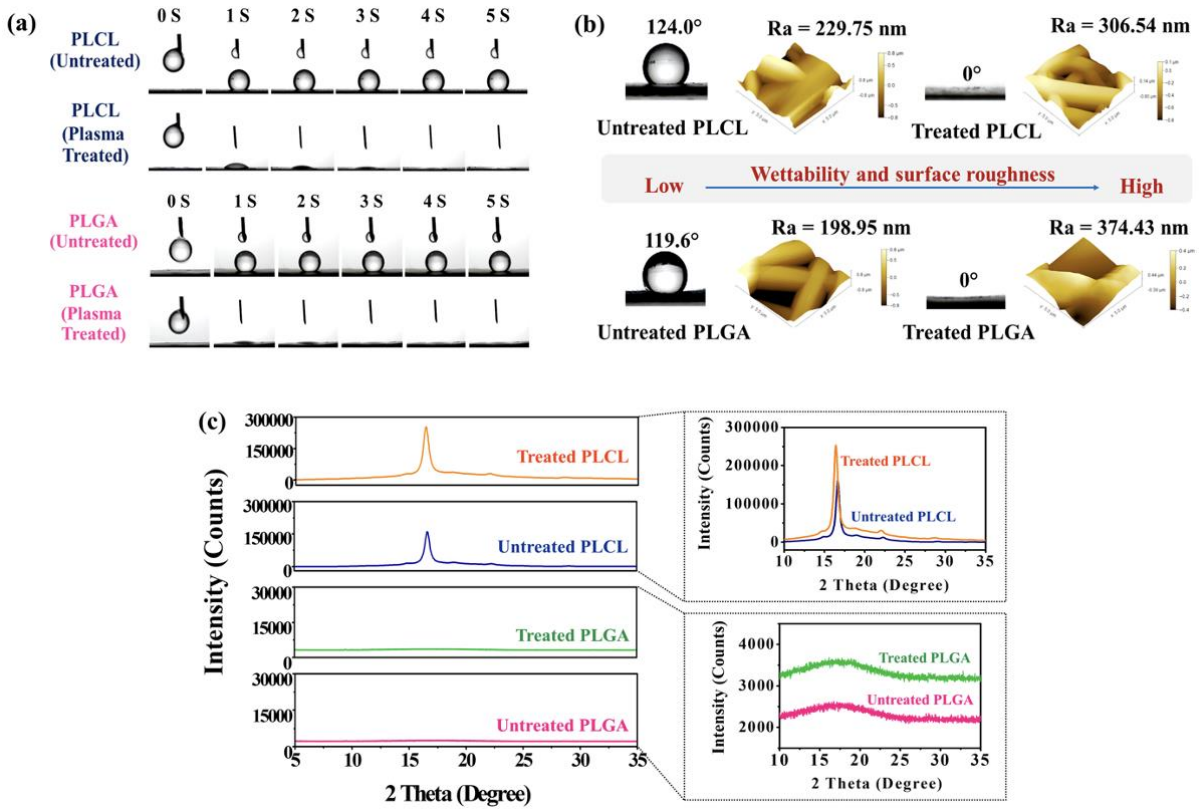

Fig. 5. (a) Absorption of water droplets on scaffolds over a 5 second period **(b)** comparison between water contact angle images and AFM images and **(c)** crystallinity of untreated and treated scaffolds (plasma treatment, 3 min at 50 W).

Figure 6 shows the curve-fitting for C_{1s}, N_{1s} and O_{1s} spectra of untreated and treated scaffolds. From the high-resolution C_{1s} spectra (Fig. 6a - b (left)), five possible carbon functional groups surface were observed on both untreated PLCL and PLGA: 1. a carbon atom bonded only to carbon or hydrogen (C-C or C-H), 2. a carbon atom with a single bond to an oxygen atom as in a hydroxyl group (C-OH) or ether group (C-O-C), 3. a carbon from a carbonyl group (C=O), 4. a carbon from an ester group (O=CO-R), 5. a carbon atom from a carboxyl group (O=C-OH) [41]. The electron binding energy of these groups could be found in untreated PLCL and PLGA scaffolds at 285.017/285.000 eV, 286.000/287.011 eV, 287.048/289.092 eV and 289.119/290.675-291.867 eV, respectively. For scaffolds treated by N_2-Ar plasma, nitrogenated carbon functional groups were also observed, which consisted of C-C or C-H at 285.051/ 284.873 eV, C-O-C or C-N at 286.421/286.355 eV, C=O at 287.311/287.295 eV, and O=CO=R (O-CO-(N,H)) at 289.090/288.983 eV. The deconvolution analysis of carbon functional groups of the surface of treated PLCL and PLGA scaffolds were significantly decreased because treatment of PLCL and PLGA surfaces with Ar can lead to

attack of the carbon bonds to form functional groups, which lead to rupture of the polymer chains.

N_2-Ar plasma activation is known to lead to N-containing functional groups, which can explain the incorporation of O-CO-N and/or C-N bonds on the PLCL and PLGA surfaces. Additionally, N_{1s} spectra demonstrate additional types of nitrogenated carbon functional groups in treated scaffolds (Fig. 6a - b (middle)). The peaks appearing at 400.172/399.062 eV and 401.815/400.250 eV were assigned to the amine group (C-N) and amide group (CONHR), respectively. The different levels of N-O and C-N in treated PLCL and PLGA scaffolds can tentatively be attributed to differences in C to O ratios in the two polymers, PLCL has a higher C to O ratio than PLGA, and therefore has more C-N than N-O. For the high-resolution O_{1s} spectra, the observed O_{1s} binding energies appeared when scaffolds were treated by N_2 and Ar, in which the new electron binding energies are observed at 533.58/533.65 and 532.23/532.22 eV (Fig. 6a - b (right)). Both treated scaffolds showed enhanced formation of nitrogen-containing bonds such as NC=O and NO-O, although it is not clear which of these were directly formed by plasma interaction with functional groups in the polymer and which were the result of post-plasma macroradical interaction with air [20,41,62]. The XPS results thus confirmed the successful outcome of N_2-Ar plasma treatment of the surfaces of PLCL and PLGA scaffolds.

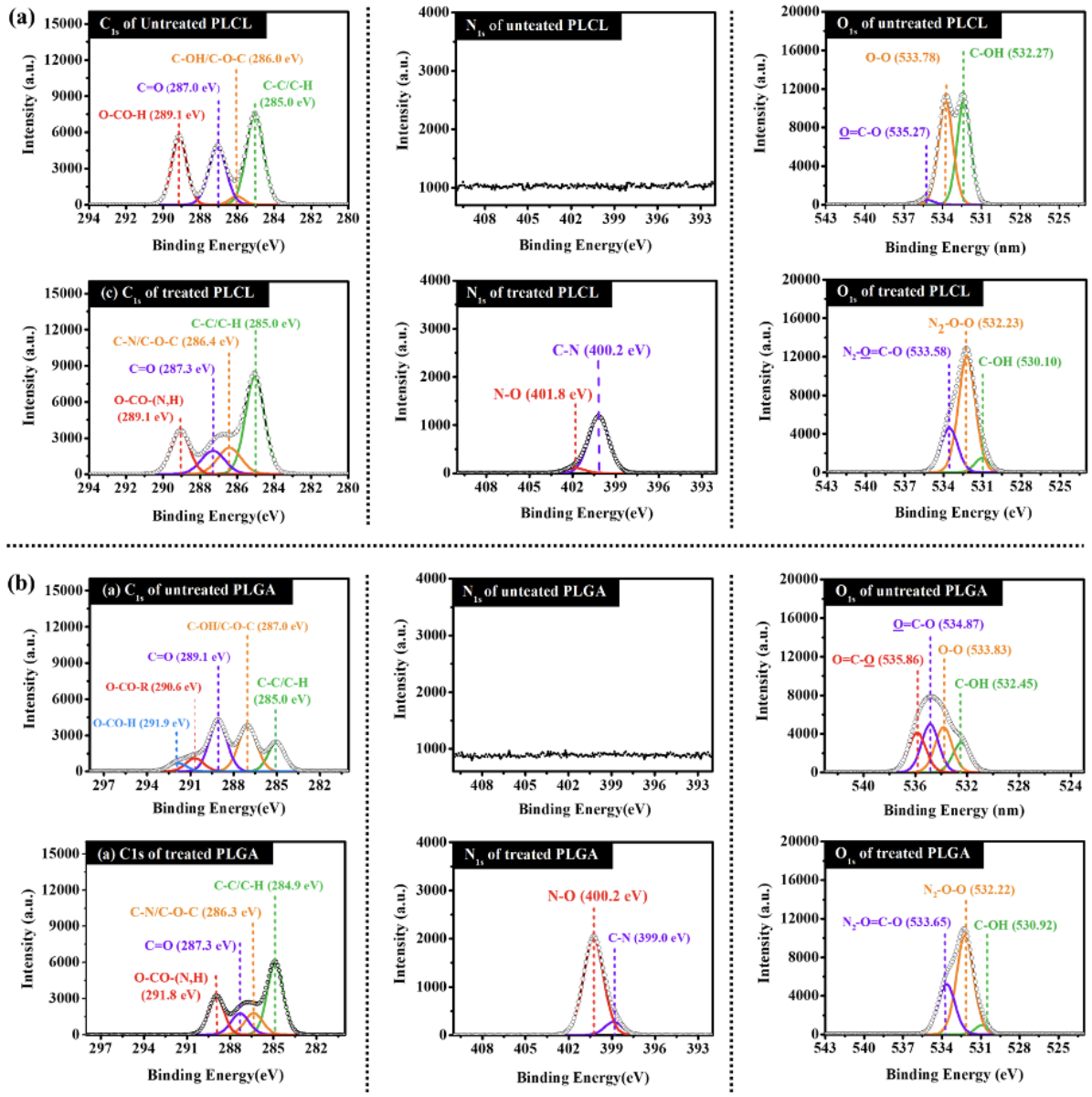

Fig. 6. High-resolution C_{1s}, N_{1s} and O_{1s} XPS spectra of untreated and treated scaffolds: (a) PLCL and (b) PLGA. (RF power 50 W, plasma treatment time 3 min).

3.3.2 Mechanical properties

As previously mentioned, we aimed to explore a composite approach to the design of scaffolds that could maintain a mechanically stable architecture and prevent collapse during the tissue regeneration process. At the same time, we believe that the scaffold should have a degree of flexibility. More flexible materials, however, are also often weaker, which might lead to kinking, breaking, and/or tearing of the suture from the scaffolds [2,6]. Therefore, it was important to characterize the mechanical properties in terms of the tensile stress-strain profile

and Young's modulus of 3D phase, E phase, untreated 3D/E and treated 3D/E scaffolds (Fig. 7).

3D phases displayed a relatively low deformation under high stress, which would lead to a stronger and stiffer scaffold, while the Young's modulus showed values of 173 ± 6 MPa (PLCL) and 397 ± 6 MPa (PLGA). A decrease in the tensile strength and Young's modulus of composite structures was observed when 3D scaffolds were combined with an E phase, due to the greater elongation of electrospun phase. It was important to observe the benefits of the composite structure, however, in that 3D/E scaffolds were much stronger than the E phase alone. Comparing the two polymer systems, 3D/E PLGA scaffolds (both untreated and treated by N_2-Ar plasma) showed higher tensile stress and Young's modulus but lower tensile strain than PLCL (both treated and untreated by N_2-Ar). This is best understood as a consequence of the greater crystallinity and higher glass transition temperature of PLGA, which behaves as a glassy material at room temperature, whereas PLCL at room temperature behaves as an elastomeric material. After plasma treatment, the tensile strength (at 1% strain) of 3D/E scaffolds of PLCL and PLGA increased due to the proportional increase in crystallinity (see Fig. 5 and Sec 3.2.2). The Young's modulus of PLCL decreased from 117 ± 8 MPa to 104 ± 6 MPa, while PLGA scaffolds increased from 410 ± 5 MPa to 446 ± 9 MPa. Moreover, it demonstrated that the mechanical characteristics of scaffolds remained rarely altered through the surface modification process. This indicated that 3D phase improved the mechanical properties of the scaffolds and made scaffolds strong enough for supporting tissue regeneration [63].

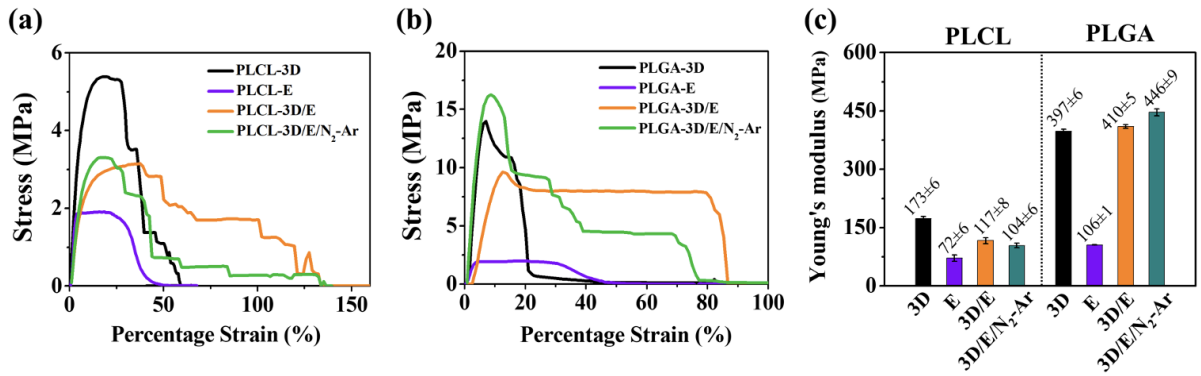

Fig. 7. Mechanical properties of untreated (3D, E and 3D/E) and treated (3D/E/N_2-Ar) scaffolds; (a) stress-strain curves of PLCL, (b) stress-strain curves of PLGA and (c) Young's modulus of PLCL and PLGA.

3.3.3 Effects of storage time

The stability of scaffolds is a particularly important property in biomedical applications. The scaffold should maintain its shape and retain its surface modified structure under in vitro conditions for a period equivalent to the repair time following tissue injury. Such in vitro studies form an important understanding of baseline behavior, although they can give no guarantee of stability in vivo. Therefore, we investigated the effect of N_2-Ar plasma treatment on the long-term performance of the scaffolds fabricated in this work by monitoring the WCA, XPS and *in vitro* hydrolytic degradation behaviors for 168 days (Fig. 8).

The water contact angle of each scaffold was measured after elapsed time periods ranging from 0 - 168 days (Fig. 8a,b). The WCA of untreated PLCL and PLGA scaffolds were 124.0 ± 1.8° and 119.6 ± 1.4°, respectively, which define them as hydrophobic materials (WCA > 90°) [64]. After N_2-Ar plasma treatments, the WCA of all scaffolds decreased to 0° within 3 s and remained at 0° after storage for 168 days, which clearly indicates a persistent increase in surface hydrophilicity (see Sec 3.2.2 for detailed comment).. Absorptivity decreased gradually when scaffolds were stored for longer time periods, as characterized by an increase in absorption time (Fig. 8c). The increase in absorption times of the water droplet was 3 s to; 4.32 ± 0.26 s (PLCL scaffold) and 3.00 ± 0.00 s (PLGA scaffold) after 7 days, 6.78 ± 0.11 s (PLCL scaffold) and 4.46 ± 0.06 s (PLGA scaffold) after 28 days, 17.89 ± 0.22 s (PLCL scaffold), 10.51 ± 1.19 s (PLGA scaffold) after 84 days and 29.94 ± 1.99 s (PLCL scaffold) and 19.23 ± 1.25 (PLGA scaffold) after 168 days.

In addition, the stability of scaffolds after treatment was also observed by the N content on the surface of treated PLCL and PLGA scaffolds during storage (Fig. 8d). After 7 days, the percentage of N content on treated PLCL and PLGA surface decreased rapidly from a relative value of 100% to 66 % and 76 %, respectively. After storage time for up to 28 days, the percentage of N content was 58 % (PLCL scaffold) and 63 % (PLGA scaffold) after 84 days, 53 % (PLCL scaffold) and 56 % (PLGA scaffold) after 168 days, 43 % (PLCL scaffold) and 49 % (PLGA scaffold). The degradation profiles of PLCL and PLGA were also observed as weight retention at temperature of 37.0 ± 1.0 °C for 0 - 168 days (Fig. 8e). The % weight retention of untreated and treated PLCL scaffolds was about 98 - 95 % (after 28 days), 90 - 75 % (after 84 days) and 60 - 45 % (after 168 days). For untreated and treated PLGA scaffolds, the % weight retention was around 85 % (after 28 days), dramatically decreased to around 35 % (after day 84) and dropped to approximately 25 % (after day 168). The degradation profiles of PLGA scaffolds with and without plasma treatment decreased more than that of PLCL scaffolds. In addition, both plasma treated scaffolds of PLCL and PLGA showed less weight retention than their untreated scaffolds. These results are consistent with the known effects of

increases in surface area (surface roughness) and surface functional group concentration due to chain scission in aliphatic polyesters [65,66].

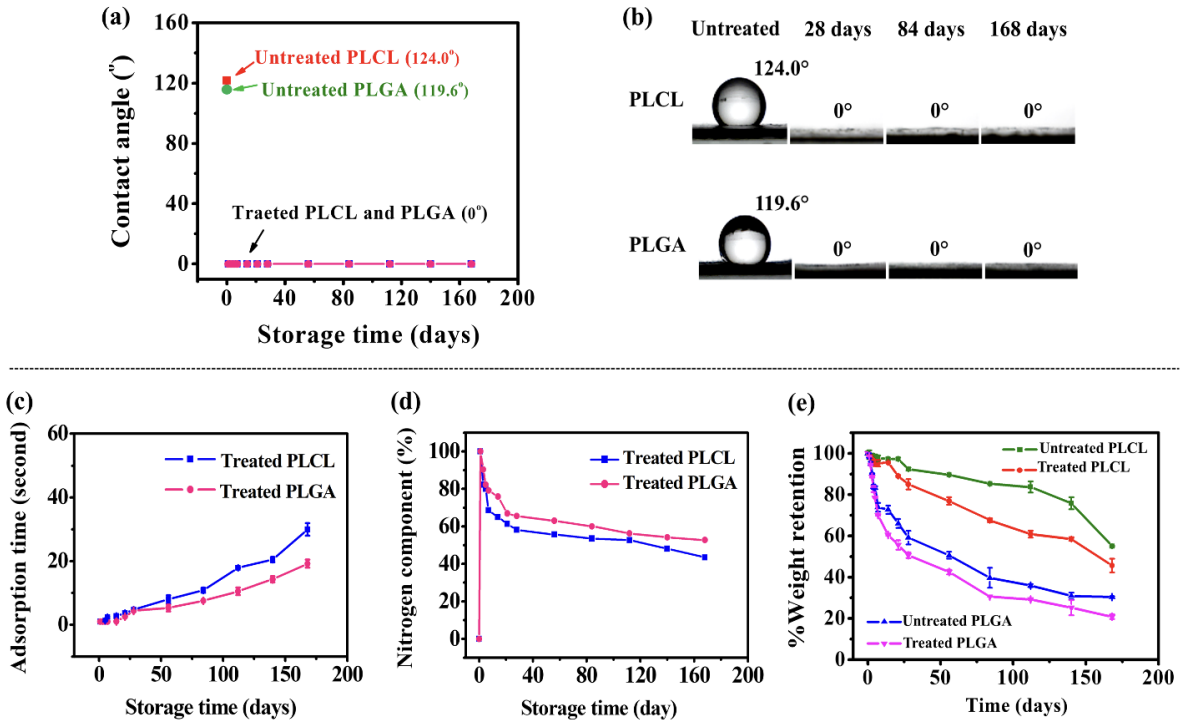

Fig. 8. Changes in surface wettability for both scaffolds (PLCL and PLGA) over 168 days following plasma treatment: (a) and (b) static water contact angle and sliding angle data of a water droplet on untreated and treated surfaces, (c) absorbing properties of a water droplet on treated surfaces, (d) nitrogen component on treated surfaces, (e) *in vitro* hydrolytic degradation of untreated and treated scaffolds.

3.3.4 Cytocompatibility testing

Cell proliferation and cell attachment

To confirm the cell-substrate interactions on treated PLCL and PLGA scaffolds, cell proliferation and cell attachment assays of SCs were performed at 1, 3, 5 and 7 days after cell seeding (Fig. 9). The percentage of cell proliferation of treated scaffolds relatively increased on the first day (Fig. 9a). One week after seeding, the SCs showed the highest attachment on the treated scaffold. In addition, the cells were well spread and grew as well as those observed on the control, as displayed in Fig. 9b. Importantly, greater cell proliferation and cell

attachment was seen on the PLGA treated scaffolds, possibly due to the higher surface roughness values induced by plasma. The E phase of both 3D/E scaffolds provided an appropriate pore size (0.253 ± 0.016 μm for PLCL and 0.238 ± 0.025 μm for PLGA), to promote better cell proliferation as compared to the 3D printed alone.

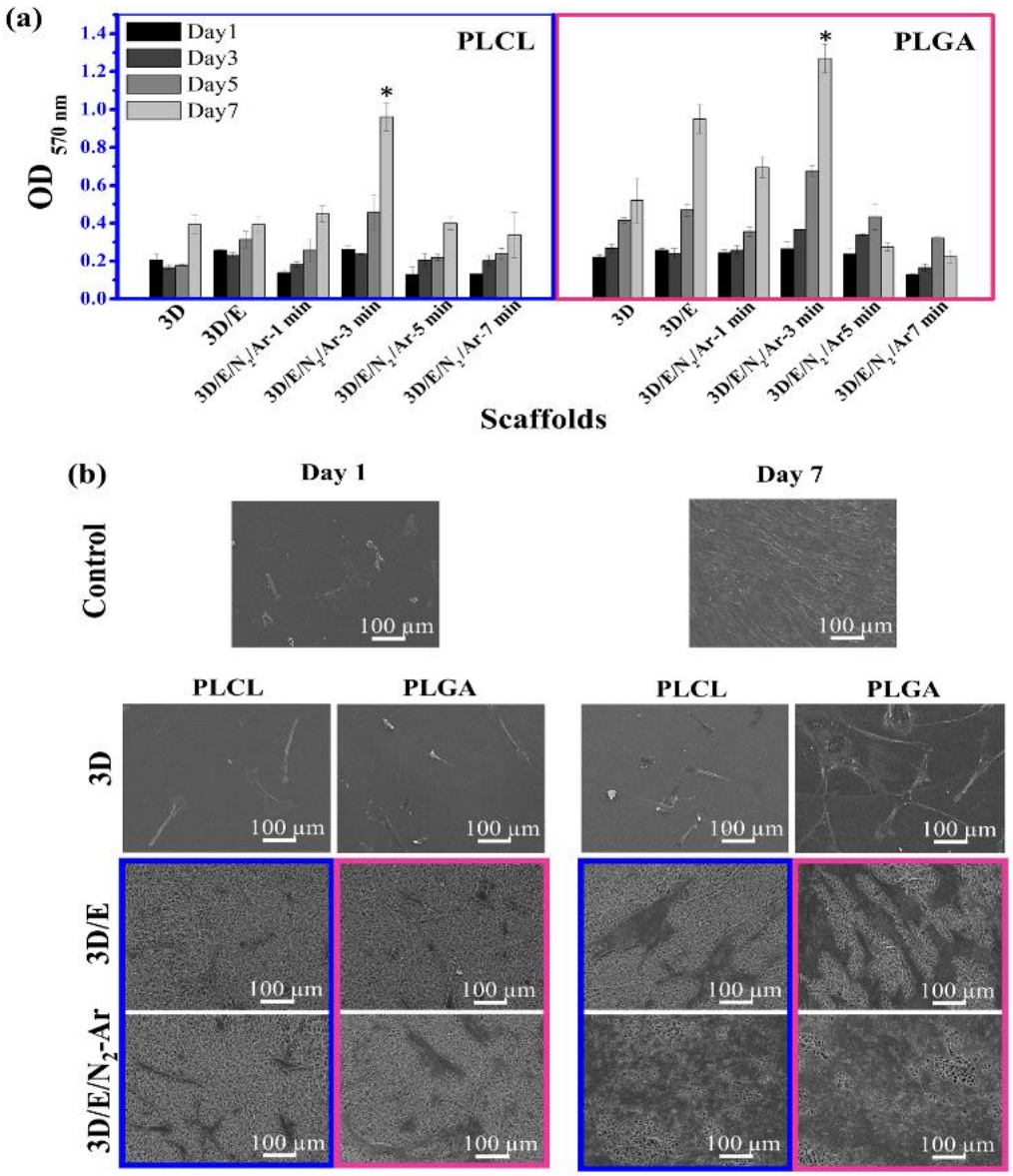

Fig. 9. Direct *in vitro* cytotoxicity of untreated and treated (PLCL and PLGA) scaffolds of the MTT assay: (a) cell proliferation of SCs and (b) cell attachment of SCs.

LHD assay

To confirm the cytocompatibility of the scaffolds, an LDH assay was carried out (to analyze the LDH release from damaged cells). Wnen the cell membranes are damaged, LDH release into the extracellular environment occurst. The release of LDH into the medium

represents an indication of cytotoxicity within the cell population [59,60,67]. Figure 10a demonstrates that the concentration of LDH released from cells cultivated on all untreated and treated scaffolds (both PLCL and PLGA) significantly increased from day 1 to day 7 (indicating an increase in cytotoxicity). All PLGA scaffolds exhibited a considerably lower concentration of LDH release than that of PLCL scaffolds. Comparing the LDH release between 3D, 3D/E and 3D/E/N_2-Ar (treated) scaffold of PLCL and PLGA; 3D/E showed higher LDH release than 3D, but lower than the plasma-treated scaffolds. This is apparently due to the fact that the E phase leads to enhanced cell proliferation (see Fig. 9), and thus an increase in the level of LDH release. Once scaffolds were treated by plasma for 3 min (see Fig. 9), not only the cell attachment and cell proliferation increased but also cell adhesion and residence (with high surface roughness). This causes less cell membrane damage (more healthy cells), resulting in a decrease in LDH release. Thus, the results clearly show that surface modification of treated scaffolds by N_2-Ar plasma plays a crucial role in improving biological performance of cells.

Apoptotic assay

To confirm the viability of cells cultivated on the untreated and treatedscaffolds (both PLCL and PLGA) at day 7, it is appropriate to examine programmed cell death (apoptosis) using Annexin V-APC/DAPI. This approach was used to observe the early- and late-stage of apoptosis (Fig. 10b), and caspase-3 activity to observe mid-stage apoptosis (Fig. 10c). Annexin V conjugated with APC is a calcium-dependent phospholipid binding protein that shows interaction with phospholipid phosphatidylserine (PS) and can be used to detect after outer membrane permeability during the early-stage of apoptosis. DAPI is a dye that can be used as a marker to determine the nuclear changes and assess late-stage apoptotic changes. Mid-stage apoptosis can be detected using caspase-3 activity, which relates to crucial mediators of the release of caspase-3 in cell lysates, resulting in destruction of cellular structures [60,68,69]. Comparing responses to, scaffolds fabricated from PLCL and PLGA, the % relative populations indicating early-, mid- and late-stage apoptosis of cells on PLGA scaffolds was slightly lower than that of PLCL scaffolds. The cell death process in early- and late-stage apoptosis on 3D/E scaffolds of both PLCL and PLGA was higher than that of 3D and 3D/E/N_2-Ar, respectively (Fig. 10b). The caspase-3 activity of treated scaffolds significantly decreased on both treated PLCL and PLGA scaffolds when compared with untreated materials (Fig. 10c). These findings corroborate those obtained from LHD release values, wherein the E phase demonstrated a greater capacity for cellular proliferation and mortality. Moreover, plasma

treatment facilitated the proliferation of healthier cells while promoting enhanced surface roughness favorable to successful entrapment and adhesion without compromising cellular integrity.

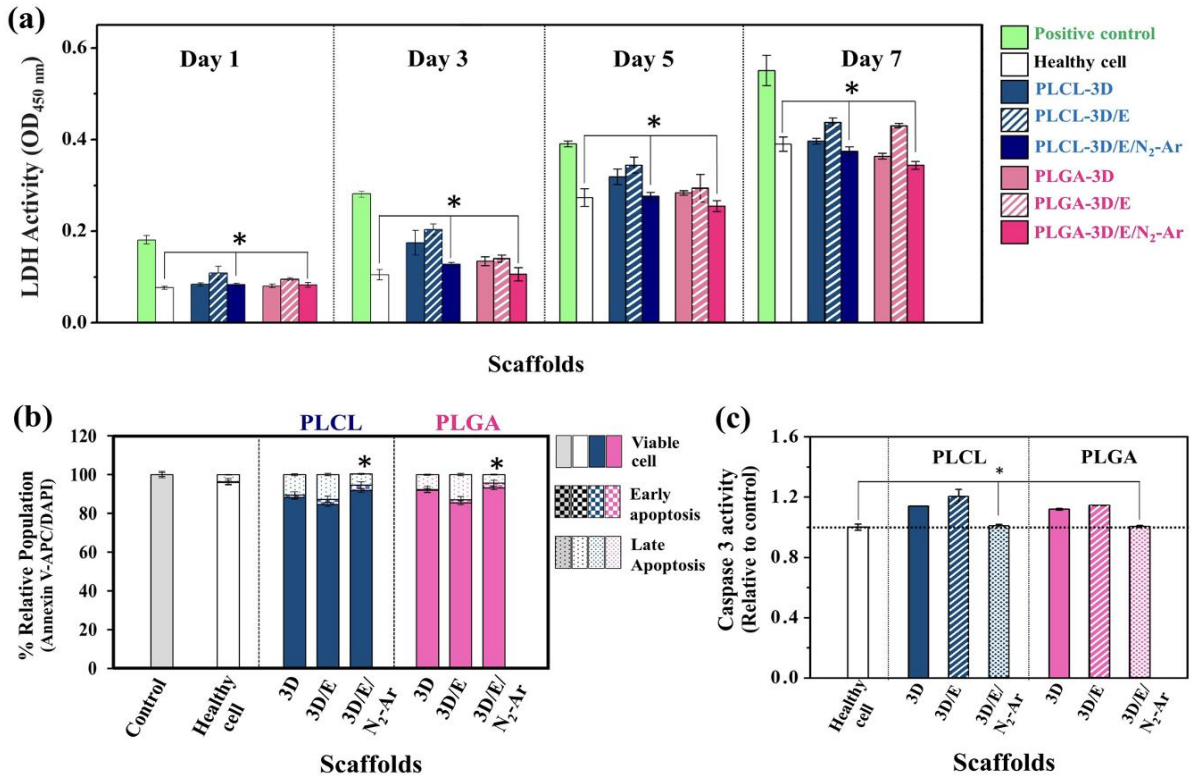

Fig. 10. Percentages of relative populations of SCs: (a) LHD assay, (b) apoptotic indices by Annexin V-APC/DAPI and (c) apoptotic indices by caspase-3 activity (*P < 0.05 compared with healthy cells).

4. CONCLUSIONS

The fabrication of two-component composite scaffolds consisting of a 3D-printed and an electrospun fiber component using poly(lactic-*co*-glycolic acid) (PLGA) and poly(lactide-*co*-*ε*-caprolactone) (PLCL) was successfully achieved. N_2-Ar plasma treatment was applied to the electrospun fiber phase, resulting in increased surface polar functional groups and oxygenation. The mechanical properties of the 3D phase were sufficient to support the scaffolds, while the electrospun fiber phase acted as the extracellular matrix (ECM) to facilitate cell attachment and proliferation. The modified surface of the electrospun fiber phase significantly improved surface wettability, leading to enhanced cell attachment, viability, proliferation, and healthy cells. Both PLGA and PLCL scaffolds demonstrated the potential for supporting cell regeneration, with PLGA performing slightly better but degrading faster and exhibiting lower strain percentage than PLCL. The scaffolds appear to have the potential for use in clinically

relevant biomedical applications, such as nerve guide conduits and nerve protectant wraps. Furthermore, the scaffolds were able to fold to diameters within the range of commercially available Food and Drug Administration (FDA)-approved products without breaking or detachment of the electrospun fiber phase. These findings suggest that these novel scaffolds hold promise for advancing regenerative medicine.

5. ACKNOWLEDGEMENTS

This work was supported by a scholarship under The Royal Golden Jubilee for a Ph.D. Program (PHD/0026/2559) and National Research University Project (NRU). The authors would like to thank the Department of Chemistry, Chiang Mai University, for providing the research facilities and the printed electronic for fabrication by the National Electronics and Computer Technology Center (NECTEC), NSTDA for financial support. This project was also partially funded from the European Union's Horizon 2020 research and innovation program under the Marie Sklodowska-Curie grant agreement no. 871650 (MEDIPOL).

6. REFERENCES

[1] M. P. Nikolova and M. S. Chavali, Recent advances in biomaterials for 3D scaffolds: A review, Bioact. Mater. 4 (2019), 271–292. https://doi.org/10.1016/j.bioactmat.2019.10.005.

[2] P. Sensharma, G. Madhumathi, R. D. Jayant, and A. K. Jaiswal, Biomaterials and cells for neural tissue engineering: Current choices, Mater. Sci. Eng. C. 77 (2017), 1302–1315. https://doi.org/10.1016/j.msec.2017.03.264.

[3] P. Kumkun, N. Tuancharoensri, G. Ross, S. Mahasaranon, J. Jongjitwimol, P. D. Topham, and S. Ross, Green fabrication route of robust, biodegradable silk sericin and poly(vinyl alcohol) nanofibrous scaffolds, Polym. Int. 68 (11) (2019), 1903–1913. https://doi.org/10.1002/pi.5900.

[4] A. Kongprayoon, G. Ross, N. Limpeanchob, S. Mahasaranon, W. Punyodom, P. D. Topham, and S. Ross, Bio-derived and biocompatible poly(lactic acid)/silk sericin nanogels and their incorporation within poly(lactide-*co*-glycolide) electrospun nanofibers, Polym. Chem. 13 (2) (2022), 3343–3357.

https://doi.org/10.1039/d2py00330a.

[5] N. Tuancharoensri, G. Ross, W. Punyodom, S. Mahasaranon, J. Jongjitwimol, P. D. Topham, and S. Ross, Multifunctional core–shell electrospun nanofibrous fabrics of poly(vinyl alcohol)/silk sericin (core) and poly(lactide-*co*-glycolide) (shell), Polym. Int. 71 (3) (2022), 266–275. https://doi.org/10.1002/pi.6319.

[6] S. Kehoe, X. F. Zhang, and D. Boyd, FDA approved guidance conduits and wraps for peripheral nerve injury: A review of materials and efficacy, Injury. 43 (5) (2012), 53–572. https://doi.org/10.1016/j.injury.2010.12.030.

[7] D. Poddar and P. Jain, Surface modification of three-dimensional porous polymeric scaffolds in tissue engineering applications: A focus review on physical modifications methods, Polym Plast Technol Eng. 61 (12) (2022), 1308–1333. https://doi.org/10.1080/25740881.2022.2061863.

[8] S. Ross, M. Yooyod, N. Limpeanchob, S. Mahasaranon, N. Suphrom, and G. M. Ross, Novel 3D porous semi-IPN hydrogel scaffolds of silk sericin and poly(N-hydroxyethyl acrylamide) for dermal reconstruction, Express Polym. Lett. 11 (9) (2017), 719–730. https://doi.org/10.3144/expresspolymlett.2017.69.

[9] N. Tuancharoensri, G. M. Ross, S. Mahasaranon, P. D. Topham, and S. Ross, Ternary blend nanofibres of poly(lactic acid), polycaprolactone and cellulose acetate butyrate for skin tissue scaffolds: influence of blend ratio and polycaprolactone molecular mass on miscibility, morphology, crystallinity and thermal properties, Polym. Int. 66 (11) (2017), 1463–1472. https://doi.org/10.1002/pi.5393.

[10] M. Yooyod, G. M. Ross, N. Limpeanchob, N. Suphrom, S. Mahasaranon, and S. Ross, Investigation of silk sericin conformational structure for fabrication into porous scaffolds with poly(vinyl alcohol) for skin tissue reconstruction, Eur. Polym. J. 81 (2016), 43–52. https://doi.org/10.1016/j.eurpolymj.2016.05.023.

[11] R. Song, M. Murphy, C. Li, K. Ting, C. Soo, and Z. Zheng, Current development of biodegradable polymeric materials for biomedical applications, Drug Des Devel Ther. 12 (2018), 3117–45. https://doi.org/10.2147/DDDT.S165440.

[12] D. Pappalardo, T. Mathisen, and A. F. Wistrand, Biocompatibility of resorbable polymers: a historical perspective and framework for the future, Biomacromolecules.

20 (4) (2019), 1465–77. https://doi.org/10.1021/acs.biomac.9b00159.

[13] I. Manavitehrani, A. Fathi, H. Badr, S. Daly, A. N. Shirazi, and F. Dehghani, Biomedical applications of biodegradable polyesters, Polymers (Basel). 8 (1) (2016), 30979116. https://doi.org/10.3390/polym8010020

[14] S. Ross, P. D. Topham, and B. J. Tighe, Identification of optically clear regions of ternary polymer blends using a novel rapid screening method, Polym. Int. 63 (1) (2014), 44–51. https://doi.org/10.1002/pi.4512.

[15] V. K. Bhovi, S. P. Melinmath, and R. Gowda, Biodegradable polymers and their applications: a rview, Adv Healthc Mater. 5 (21) (2016), 2732–44. https://doi.org/ 10.2174/1389557522666220128152847.

[16] G. Ross, S. Ross, and B. J. Tighe, Bioplastics: New Routes, New Products. Brydson's Plastics Materials, 8th ed.; Elsevier, (2017), 631–652. https://doi.org/10.1016/B978-0-323-35824-8.00023-2.

[17] P. Chen, Z. Zhou, W. Liu, Y. Zhao, T. Huang, X. Li, J. Duan, and F. Fang, Preparation and Characterization of Poly(L-lactide-*co*-glycolide-*co*-*ε*-caprolactone) Scaffolds by Thermally Induced Phase Separation, J. Macromol. Sci. Part B Phys. 59 (7) (2020), 427–439. https://doi.org/10.1080/00222348.2020.1735136.

[18] S. I. Kim, J. I. Lim, Y. Jung, C. H. Mun, J. H. Kim, and S. H. Kim, Preparation of enhanced hydrophobic poly(l-lactide-*co*-*ε*-caprolactone) films surface and its blood compatibility, Appl. Surf. Sci. 276 (2013), 586–591. https://doi.org/10.1016/j.apsusc.2013.03.137.

[19] X. Sun, C. Xu, G. Wu, Q. Ye, and C. Wang, Review poly(lactic-co-glycolic acid): Applications and future prospects for periodontal tissue regeneration, Polymers. 9 (6). (2017), 189. https://doi.org/10.3390/polym9060189.

[20] R. Vasita, K. Shanmugam, and D. S. Katti, Improved Biomaterials for Tissue Engineering Applications: Surface Modification of Polymers, Curr. Med. Chem. 8 (2008), 341–353. https://doi.org/10.2174/156802608783790893.

[21] H. S. Yoo, T. G. Kim, and T. G. Park, Surface-functionalized electrospun nanofibers for tissue engineering and drug delivery, Adv. Drug Deliv. Rev. 61 (12) (2009), 1033–1042. https://doi.org/10.1016/j.addr.2009.07.007.

[22] S. Ross, S. Mahasaranon, and G. M. Ross, Ternary polymer blends based on poly(lactic acid): Effect of stereo-regularity and molecular weight, J. Appl. Polym. Sci. 132 (14) (2015), 1–8. https://doi.org/10.1002/app.41780.

[23] E. Biazar, M. Kamalvand, and F. Avani, Recent advances in surface modification of biopolymeric nanofibrous scaffolds, Int. J. Polym. Mater. Polym. Biomater. 71 (7) (2022), 493–512. https://doi.org/10.1080/00914037.2020.1857383.

[24] R. Morent, N. De Geyter, T. Desmet, P. Dubruel, and C. Leys, Plasma surface modification of biodegradable polymers: A review, Plasma Process. Polym. 8 (3), (2011), 171–190. https://doi.org/10.1002/ppap.201000153.

[25] L. Cheng, R. Ghobeira, P. Cools, Z. Liu, K. Yan, N. D. Geyte, and R. Morent, Comparative study of different nitrogen-containing plasma modifications applied on 3D porous PCL scaffolds and 2D PCL films, Appl. Surf. Sci. 516 (2020), 146067. https://doi.org/10.1016/j.apsusc.2020.146067.

[26] J. Wang, N. Chen, S. Ramakrishna, L. Tian, and X. Mo, The effect of plasma treated PLGA/MWCNTs-COOH composite nanofibers on nerve cell behavior, Polymers. 9 (12) (2017), 713. https://doi.org/10.3390/polym9120713.

[27] T. Y. Bak, M. S. Kook, S. C. Jung, and B. H. Kim, Biological effect of gas plasma treatment on CO2 gas foaming/salt leaching fabricated porous polycaprolactone scaffolds in bone tissue engineering, J. Nanomater. 2014 (2014), 1–6. https://doi.org/10.1155/2014/657542.

[28] P. Cools, M. Asadian, W. Nicolaus, H. Declercq, R. Morent, and N. De Geyter, Surface treatment of PEOT/PBT (55/45) with a dielectric barrier discharge in air, helium, argon and nitrogen at medium pressure, Materials. 11 (3) (2018), 1–15. https://doi.org/10.3390/ma11030391.

[29] S. Tunma, K. Inthanon, C. Chaiwong, J. Pumchusak, W. Wongkham, and D. Boonyawan, Improving the attachment and proliferation of umbilical cord mesenchymal stem cells on modified polystyrene by nitrogen-containing plasma, Cytotechnology, 65 (1) (2013), 119–134. https://doi.org/10.1007/s10616-012-9467-9.

[30] P. Favia and R. D'Agostino, Plasma treatments and plasma deposition of polymers for biomedical applications, Surf. Coatings Technol. 98 (1998), 1102–1106.

https://doi.org/10.1016/S0257-8972(97)00285-5.

[31] P. K. Chu, J. Y. Chen, L. P. Wang, and N. Huang, Plasma-surface modification of biomaterials, Mater. Sci. Eng. R Reports. 36 (5–6) (2002), 143–206. https://doi.org/10.1016/S0927-796X(02)00004-9.

[32] J. M. Grace and L. J. Gerenser, Plasma treatment of polymers, Dispers. Sci. Technol. 24 (3–4) (2003). 305–341, https://doi.org/10.1081/DIS-120021793.

[33] A. Kumar, and A. Jacob Techniques in scaffold fabrication process for tissue engineering applications: a review, J Appl Biol Biotechnol. 10 (3) (2022), 163–76. https://doi.org/10.7324/JABB.2022.100321.

[34] B. Subia, J. Kundu, and S. C. Kundu, Biomaterial scaffold fabrication techniques for potential tissue engineering applications, Tissue Eng, (2010), 141–158. https://doi.org/10.5772/8581.

[35] J. Ding, J. Zhang, J. Li, D. Li, C. Xiao, H. Xiao, H. Yang, X. Zhuang, and X. Chen, Electrospun polymer biomaterials, Prog Polym Sci. 90 (2019), 1–34. https://doi.org/10.1016/j.progpolymsci.2019.01.002.

[36] X. Feng, J. Li, X. Zhang, T. Liu, J. Ding, and X. Chen, Electrospun polymer micro/nanofibers as pharmaceutical repositories for healthcare, J Control Release. 302 (2019), 19–41. https://doi.org/10.1016/j.jconrel.2019.03.020.

[37] J. J. Chung, H. Im, S. H. Kim, J. W. Park, and Y. Jung, Toward biomimetic scaffolds for tissue engineering: 3D printing techniques in regenerative medicine, Front Bioeng Biotechnol. 8 (2020), 1–12. https://doi.org/10.3389/fbioe.2020.586406.

[38] S. Vijayavenkataraman, S. Thaharah, S. Zhang, W. F. Lu, and J. Y. H. Fuh, Electrohydrodynamic jet 3D-printed PCL/PAA conductive scaffolds with tunable biodegradability as nerve guide conduits (NGCs) for peripheral nerve injury repair, Mater. Des. 162 (2019), 171–184. https://doi.org/10.1016/j.matdes.2018.11.044.

[39] Y. W. D. Tay, M. Y. Li, and M. J. Tan, Effect of printing parameters in 3D concrete printing: Printing region and support structures, J. Mater. Process. Technol. 271 (2019), 261–270. https://doi.org/10.1016/j.jmatprotec.2019.04.007.

[40] Y. Liu, X. Liang, A. Saeed, W. Lan, and W. Qin, Properties of 3D printed dough and

optimization of printing parameters, Innov. Food Sci. Emerg. Technol. 54 (2019), 9–18. https://doi.org/10.1016/j.ifset.2019.03.008.

[41] P. Techaikool, D. Daranarong, J. Kongsuk, D. Boonyawan, N. Haron, W. S. Harley, K. A. Foster, L. J. R. Foster, and W. Punyodom, Effects of plasma treatment on biocompatibility of poly[(L-lactide)-*co*-(*ε*-caprolactone)] and poly[(L-lactide)-co-glycolide] electrospun nanofibrous membranes, Polym. Int. 66 (11) (2017), 1640–1650. https://doi.org/10.1002/pi.5427.

[42] Z. Rao, Z. Lin, P. Song, D. Quan, and Y. Bai. Biomaterial-based schwann cell transplantation and schwann cell-derived biomaterials for nerve regeneration, Front Cell Neurosci. 16 (2022), 1–18. https://doi.org/10.3389/fncel.2022.926222.

[43] G. Nocera, and C. Jacob, Mechanisms of schwann cell plasticity involved in peripheral nerve repair after injury, Cell Mol Life Sci. 77 (20) 2020, 3977–3989. https://doi.org/10.1007/s00018-020-03516-9.

[44] Y. Li, C. Wu, Y. Bai, S. Lui, C. Yuan, T. Ding, and Y. Hu, Effect of glow discharge plasma on surface modification of chitosan film, Int. J. Biol. Macromol. 138 (2019), 340–348. https://doi.org/10.1016/j.ijbiomac.2019.07.039.

[45] D. Gogoi, A. J. Choudhury, J. Chutia, A. R. Pal, N. N. Dass, D. Devi, and D. S. Patil, Enhancement of hydrophobicity and tensile strength of muga silk fiber by radiofrequency Ar plasma discharge, Appl. Surf. Sci. 258 (1) (2011), 126–135. https://doi.org/10.1016/j.apsusc.2011.08.018.

[46] T. Paragkumar, D. Edith, and S. Jean-Luc, Surface characteristics of PLA and PLGA films, Appl. Surf. Sci. 253 (2006), 2758-2764.

https://doi.org/10.1016/j.apsusc.2006.05.047

[47] Z. Qi, W. Guo, S. Zheng, C. Fu, Y. Ma, S. Pan, Q. Liu, and X. Yang, Enhancement of neural stem cell survival, proliferation and differentiation by IGF-1 delivery in graphene oxide-incorporated PLGA electrospun nanofibrous mats, RSC Adv. 9 (2019), 8315-8325.

https://doi.org/10.1039/C8RA10103E

[48] T. Jacobs, N. D. Geyter, R. Morent, T. Desmet, P. Dubruel, and C. Leys, Plasma

treatment of polycaprolactone at medium pressure, Surf. Coat. Technol. 205 (2011), S543–S547

https://doi.org/10.1016/j.surfcoat.2011.02.012

[49] R. N. wenzel, Surface Roughness and Contact Angle, J. Phys. Chem. 53(9) (1949), 1466–1467.

https://doi.org/10.1021/j150474a015

[50] A.B.D. Cassie, and S. Baxter, Wettability of porous surfaces, Trans. Faraday Soc. 40 (1982), 546-551.

https://doi.org/10.1039/TF9444000546

[51]. S. Wu, “Polymer Interface and Adhesion” Marcel Dekker Inc, New York 1982, pp 16-26.

https://doi.org/10.1201/9780203742860

[52] H. Yasuda, H. C. Marsh, E. S. Brandt, and C. N. Reilley, ESCA study of polymer surfaces treated by plasma. J. Polym. Sci. Polym. Chem. Ed., 15 (1977), 991-1019.

https://doi.org/10.1002/pol.1977.170150420

[53]. M. Hudis, "Techniques and applications of plasma chemistry." edited by JR Hollahan, AT Bell, John Willy & Sons, Inc., New York (1974): 113.

https://doi.org/10.1002/pol.1975.130130317

[54] F. D. Denes, and S. Manolache, Macromolecular plasma-chemistry: an emerging field of polymer science, Prog.Polym.Sci. 29(8) (2004), 815-885.

https://doi.org/10.1016/j.progpolymsci.2004.05.001

[55]. A.E. Wiacek, K. Terpilowski, M. Jurak, and M. Worzakowska, Effect of low-temperature plasma on chitosan-coated PEEK polymer characteristics, Eur. Polym. J. 78 (2016), 1-13.

https://doi.org/10.1016/j.eurpolymj.2016.02.024

[56] D. Briggs, and J.T. Grant (eds). Surface analysis by Auger and x-ray photoelectron spectroscopy, IM Publications, Chichester, UK, 2003, 900 pp., ISBN 1-901019-04-7, 900 pp.

https://doi.org/10.1002/sia.2005

[57] Y. Li, J. H. Kim, E. H. Choi, and I. Han, Promotion of osteogenic differentiation by non-thermal biocompatible plasma treated chitosan scaffold, Sci. Rep. 9 (2019), 3712. https://doi.org/10.1038/s41598-019-40371-6.

[58] P. Taylor, E. D. Yildirim, R. Besunder, S. Guceri, F. Allen, and W. Sun, Fabrication and plasma treatment of 3D polycaprolactane tissue scaffolds for enhanced cellular function, Virtual Phys. Prototyp. 3 (4) (2008), 199–207. https://doi.org/10.1080/17452750802547338.

[59] B. S. Cummings and R. G. Schnellmann, Measurement of Cell Death in Mammalian Cells, Curr. Protoc. 1 (8) (2021). https://doi.org/10.1002/cpz1.210.

[60] G. Banfalvi, Methods to detect apoptotic cell death, Apoptosis. 22 (2) (2017), 306–323. https://doi.org/10.1007/s10495-016-1333-3.

[61] Y. Yuan and T. R. Lee, Contact angle and wetting properties, Springer Ser. Surf. Sci. 51 (1) (2013), 3–34. https://doi.org/10.1007/978-3-642-34243-1_1.

[62] J. Yang, J. Bei, and S. Wang, Enhanced cell affinity of poly (d,l-lactide) by combining plasma treatment with collagen anchorage, Biomaterials. 23 (2002), 2607–2614. https://doi.org/10.1016/S0142-9612(01)00400-8.

[63] S. Zhang, S. Vijayavenkataraman, G. L. Chong, J. Y. H. Fuh, and W. F. Lu, Computational Design and Optimization of Nerve Guidance Conduits for Improved Mechanical Properties and Permeability, J. Biomech. Eng. 141 (5) (2019), 051007. https://doi.org/10.1115/1.4043036.

[64] S. Shafei, J. Foroughi, Z. Chen, C. S. Wong, and M. Naebe, Short oxygen plasma treatment leading to long-term hydrophilicity of conductive PCL-PPy nanofiber scaffolds, Polymers. 9 (11) (2017). https://doi.org/10.3390/polym9110614.

[65] X. H. Zong, Z. G. Wang, B. H. Hsiao, B. Chu, J. J. Zhou, D. D. Jamiolkowski, E. Muse, and E. Dormier, Structure and morphology changes in absorbable

poly(glycolide) and poly(glycolide-*co*-lactide) during in vitro degradation, Macromolecules. 32 (24) (1999), 8107–8114. https://doi.org/10.1021/ma990630p.

[66] Y. Dong, S. Liao, S. Ramakrishna, and C. K. Chan, Distinctive degradation behaviors of electrospun PGA, PLGA and P(LLA-CL) nanofibers cultured with/without cell culture, Adv Mat Res. 47-50 (2008), 1327–1330. https://doi.org/10.4028/www.scientific.net/amr.47-50.1327.

[67] D. T. Loo and J. R. Rillema, Measurement of Cell Death, Methods Cell Biol. 57 (1998), 251–264. https://doi.org/10.1016/s0091-679x(08)61583-6.

[68] M. M. Martinez, R. D. Reif, and D. Pappas, Detection of apoptosis: A review of conventional and novel techniques, Anal. Methods. 2 (8) (2010), 996–1004. https://doi.org/10.1039/c0ay00247j.

[69] M. V. Engeland, L. J. W. Nieland, F. C. S. Ramaekers, B. Schutte, and C. P. M. Reutelingsperger, annexin V-affinity assay: a review on an apoptosis detection system based on phosphatidylserine exposure, Cytometry. 31 (1998), 1–9. https://doi.org/10.1002/(SICI)1097-0320(19980101)31:1<1::AID-CYTO1>3.0.CO;2-R.